Instability of a salt jet emitted from a point source in an external electric field

Cite as: Phys. Fluids **34**, 084103 (2022); https://doi.org/10.1063/5.0098652
Submitted: 11 May 2022 • Accepted: 06 July 2022 • Published Online: 03 August 2022

S. Amiroudine, E. A. Demekhin, G. S. Ganchenko, et al.

Physics of Fluids ARTICLE scitation.org/journal/phf

Instability of a salt jet emitted from a point source in an external electric field

Cite as: Phys. Fluids **34**, 084103 (2022); doi: 10.1063/5.0098652
Submitted: 11 May 2022 · Accepted: 6 July 2022 ·
Published Online: 3 August 2022

S. Amiroudine,[1] E. A. Demekhin,[2,3,4,a)] G. S. Ganchenko,[3] V. S. Shelistov,[3] and E. A. Frants[2,3]

AFFILIATIONS

[1]Institut de Mécanique et d'Ingénierie, UMR CNRS 5295, University of Bordeaux, 351 Cours de la Libération, 33405 Talence, France
[2]Department of Mathematics and Computer Science, Financial University under the Government of the Russian Federation, Moscow 125167, Russian Federation
[3]Laboratory of Micro- and Nanoscale Electro- and Hydrodynamics, Financial University under the Government of the Russian Federation, Moscow 125167, Russian Federation
[4]Laboratory of General Aeromechanics, Institute of Mechanics, Moscow State University, Moscow 119192, Russian Federation

[a)]**Author to whom correspondence should be addressed:** edemekhi@gmail.com

ABSTRACT

The objective in the present work is to consider a simple example of instability of a conducting self-similar micro jet in the external electric field, which represents a prototype of some microfluidic instabilities. Salt from a point source is emitted into its own aquatic solution, which is subject to an external uniform velocity field together with an electrostatic field, and is convected downstream and diffused. The flow is considered in microscales so that, in contrast to the classical jets, the Reynolds numbers are practically zero, but the Péclet numbers are large. The parameters are found at which such a microjet is unstable. Along with the linear stability analysis, we have fulfilled the numerical simulations of the full nonlinear system of equations. The numerical simulation qualitatively confirmed the results of the linear stability and showed that this instability visually reminds classical instabilities of free jets and wakes.

I. INTRODUCTION

Problems of electrokinetics and micro- and nanofluidics have recently attracted a great deal of attention due to rapid developments in micro-, nano-, and biotechnology. Among the numerous modern micro- and nanofluidic applications of electrokinetics are, in particular, micromixers and microreactors. The simplest type of such a mixer or reactor is a T- or Y-shaped channel, at the entrance of which two types of liquids are supplied, and they mix due to diffusion when moving toward the outlet. There are also injection mixers, when the second liquid is directly fed from a small nozzle into the microchannel and carried away by the flow of the first liquid, also mixing with it due to diffusion. For both types, mixing is slow because it is bound by small diffusion coefficients. The process requires a long enough channel and time for complete mixing. The mixing time can be effectively reduced with the help of electrohydrodynamic instabilities.

Microscale flows occur at almost zero Reynolds numbers, and therefore, it is intuitively difficult to *a priori* expect a manifestation of any type of the hydrodynamic instability. However, experimental and theoretical studies have shown a very rich picture of instabilities and subsequent bifurcations and transitions, ultimately leading to chaotic dynamics.[1] One kind of instability in microscale flows in an electrolyte solution between ion-selective membranes under an electrical potential drop was theoretically predicted by Rubinstein and Zaltzman[2,3] and subsequently investigated numerically.[4–8] This kind of instability was experimentally confirmed in the subsequent investigations.[9–12] A new type of instability, which prevails in long microchannels, was recently addressed in our works[13,14] and experimentally confirmed by other researchers.[15] It is connected with Joule heating effects in microscales and correspond to applications in thermal engineering.[16–19]

Another kind of electrohydrodynamic instability, instability of liquid flows with conductivity gradients, stems from the pioneer works of Hoburg and Melcher,[20] in turn based on classical leaky dielectric models by Melcher and Taylor[21] (see also the works of Melcher and Saville[22,23]).

Hoburg and Melcher described[20] the key mechanism of this instability as caused by charge accumulation at a perturbed interface and made qualitative comparisons of their theory to experiments. Instead of the Nernst–Planck–Poisson system, they used a simplified approach, neglecting the diffusion terms for instance. As a result, their calculations were of a qualitative nature, in particular, the threshold of

instability could not be predicted. This disadvantage was improved by Baygents and Baldessari,[24] which made the model more realistic.

Research with this sort of electrohydrodynamic instability was continued by Santiago's team.[25–30] The flow in a long, rectangular-cross section microchannel with a conductivity gradient orthogonal to the main flow direction and an external electric field was considered both experimentally and theoretically.[26] It was found experimentally that such a system exhibits a critical electric field above which the flow is unstable. In the theoretical part the authors generalized the previous model.[24] The relation for the Helmholtz–Smoluchowski electro-osmotic velocity was used as an effective boundary condition (BC) for the bulk flow. The theory predicts both qualitative trends and quantitative features that agree very well with experimental data. Santiago's team[27–29] found that the instability is governed by two key control parameters: the ratio of dynamic to dissipative forces which governs the onset of instability and the ratio of electro-viscous to electro-osmotic velocities which governs the convective vs absolute nature of instability. It was shown that such instability can be characterized by the electric Rayleigh number which is the ratio of diffusive and electro-viscous time scales.

In the work by Posner, Perez, and Santiago,[30] a numerical investigation of chaotic dynamics of the above flow with gradient of electric conductivity in a microchannel was presented. As the electric Rayleigh number increases, a flow dynamics transition from a steady state to a regular time-periodic state and, next, to a chaotic one was shown. Further increase of the Rayleigh number leads to a transition back to the regular state followed by a second transition to the chaotic dynamics. The authors presented temporal power spectra and time-delay phase maps of low-dimensional attractors and graphically depicted the sequence between periodic and chaotic states.

In the experimental work by Dubey *et al.*,[31] an investigation of the instability with gradient of conductivity in microchannel flow was fulfilled using time-resolved visualization of a passive fluorescent scalar. The authors used dynamic mode decomposition of time-resolved snapshots of instability to investigate its spatiotemporal coherent structures for a wide range of the electric Rayleigh number. The analysis yields spatial variation of modes of instability along with their corresponding temporal frequencies; it was shown that the instability can be characterized by transverse and longitudinal coherent structures which strongly depend on the electric Rayleigh number.

There is another example of instabilities in the microscale electrohydrodynamics. The flux near the ion-selective microgranule due to its curved membrane-like surface and the tangential ion flux is prone to several kinds of instabilities.[32–34] In particular, a salt jet is formed in the region of outgoing ions, see Fig. 1. With the increasing of the external field E_∞, this jet becomes narrow and unstable.[34]

The objective of the present work is to study the behavior of a jet of salt emitted by a thin point source in an external electric field. Salt from the source is emitted into its own aquatic solution, which is subject to an external uniform velocity field and an electrostatic field, where it is convected downstream and diffused. This flow is considered in microscales, so that, in contrast to the classical jets, the Reynolds numbers are practically zero, but the Péclet numbers can be large. Such a combination is possible due to the very small ratio of the diffusion coefficient to the kinematic viscosity coefficient. This statement mimicks electrokinetic processes in applications, so we can treat the instability of such a jet as a simplest prototype of instabilities described in the above-mentioned works.[20–34] Consequently, its investigation will allow predicting instabilities in other electrohydrodynamic flows with concentration gradients.

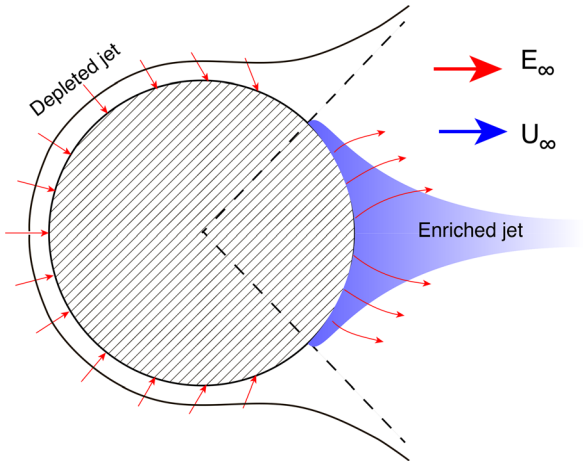

FIG. 1. Schematics for an ion-selective sphere with a single surface but different regions of the outgoing and the incoming ion fluxes. The small red arrows show the ion flux. Depleted and enriched salt areas are depicted with white and blue, respectively.

II. MATHEMATICAL FORMULATION

Let us consider a source of salt immersed into a background aquatic solution of the same salt in external uniform velocity and electrostatic fields, see Fig. 2. Notations with a tilde are used for the dimensional variables, as opposed to their dimensionless counterparts without the tilde. The salt source is situated along the straight line of length $\tilde{b}$, perpendicular to the $\tilde{x}$–$\tilde{y}$ plane. The salt is carried away by advection and spreads to the sides by diffusion, eventually forming a jet flow, as it is shown in Fig. 2.

The problem is posed for a symmetric binary electrolyte. The external electric field breaks the electrical neutrality of the jet, and the molar concentrations of anions $(\tilde{c}^-)$ and cations $(\tilde{c}^+)$ along the jet become different, $\tilde{c}^+ \neq \tilde{c}^-$. The whole problem is described by the

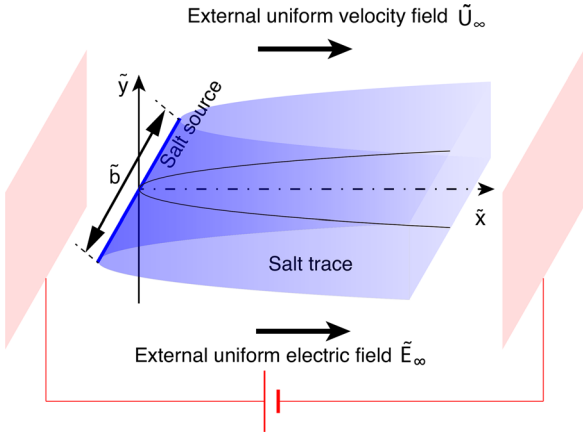

FIG. 2. Sketch of the base configuration for the well-developed jet emitted from a point source.

Nernst–Planck equations for the transport of ions, the Poisson equation for the electric potential, and the Navier–Stokes equations with the volume Coulomb force. The diffusion coefficients for the cations and anions are assumed to be equal, $\tilde{D}^+ = \tilde{D}^- = \tilde{D}$.

If we assume that the normalized difference $c_\varepsilon = (\tilde{c}^+ - \tilde{c}^-)/(\tilde{c}^+ + \tilde{c}^-)$ is small, the system of equations can be simplified to the Ohmic model. The Nernst–Planck equations in the leading-order approximation with respect to c_ε are electroneutral and can be combined to yield (see Ref. 35)

$$\begin{cases} \dfrac{\partial \tilde{K}}{\partial \tilde{t}} + \tilde{\mathbf{U}} \cdot \nabla \tilde{K} = \tilde{D}\, \nabla^2 \tilde{K} + \tilde{q}, \\ \nabla \cdot (\tilde{K} \nabla \tilde{\Phi}) = 0. \end{cases} \tag{1}$$

The first equation is the convection–diffusion equation for the molar salt concentration $\tilde{K} = \tilde{c}^+ + \tilde{c}^-$, and the second equation is the equation for the Ohmic current density $\tilde{K}\nabla\tilde{\Phi}$, where $\tilde{\Phi}$ is the electric potential and $\tilde{K}$ is proportional to the electric conductivity. Convection and diffusion currents disappear under our assumptions. For the electroneutral electrolyte, $\tilde{c}^+ = \tilde{c}^- = \tilde{c}$, which gives $\tilde{K} = 2\tilde{c}$. $\tilde{q}$ is the salt flux from the source, which can be expressed via the molar concentration flow rate of salt $\tilde{Q}$ in the following form in the Cartesian coordinate system $\tilde{x}$–$\tilde{y}$:

$$\tilde{q} = \tilde{Q} \frac{\delta(\tilde{x})\, \delta(\tilde{y})}{\tilde{b}\tilde{L}_0^2}, \tag{2}$$

where δ is the Dirac delta function (see, for example, Courant and Hilbert[36]).

In the leading order with respect to c_ε, the Navier–Stokes equations with the Coulomb force can be written as follows:

$$\begin{cases} \dfrac{\partial \tilde{\mathbf{U}}}{\partial \tilde{t}} + \tilde{\mathbf{U}} \cdot (\nabla \tilde{\mathbf{U}}) + \dfrac{1}{\tilde{\rho}} \nabla \tilde{\Pi} - \dfrac{\tilde{\mu}}{\tilde{\rho}} \nabla^2 \tilde{\mathbf{U}} = \dfrac{\tilde{\varepsilon}}{\tilde{\rho}} \nabla^2 \tilde{\Phi}\, \nabla \tilde{\Phi}, \\ \nabla \tilde{\mathbf{U}} = 0. \end{cases} \tag{3}$$

The Ohmic model was adopted in the study of the electro-diffusion process of electrolytes in many different physical regimes (the details of derivation can be found elsewhere[27]). This model is accurate because the difference in cationic and anionic concentrations is very small compared to the background concentration of electrolytes, but this difference is strong enough to promote instability via electric body forces.

Far from the origin, the velocity and electric fields tend to their unperturbed values and the salt concentration tends to its background value

$$\tilde{x}^2 + \tilde{y}^2 \to \infty: \quad \tilde{U} \to \tilde{U}_\infty, \quad \tilde{V} \to 0, \quad \tilde{K} \to 2\tilde{c}_\infty, \quad \frac{\partial \tilde{\Phi}}{\partial \tilde{x}} \to -\tilde{E}_\infty, \tag{4}$$

where $\tilde{\mathbf{U}} = (\tilde{U}, \tilde{V})$ and $\tilde{U}$ is directed along the $\tilde{x}$-axis and $\tilde{V}$ is directed along $\tilde{y}$-axis.

At the initial time, all the fields are unperturbed

$$\tilde{K} = 2\tilde{c}_\infty, \quad \tilde{U} = \tilde{U}_\infty, \quad \tilde{V} = 0, \quad \tilde{\Phi} = -\tilde{E}_\infty \tilde{x}. \tag{5}$$

Spatial nonuniformity of the salt concentration causes the nonuniformity of the electric conductivity and, therefore, induces the volume Coulomb forces appearing in the momentum balance equations. Originally uniform, the electric, the velocity, and the concentration fields are becoming deformed, and these deformations may lead to the electrohydrodynamic instability. The main objective of the present work is to study and explain this instability.

The characteristic quantities to make the system dimensionless are as follows:

- $\tilde{U}_0 = \tilde{U}_\infty$ is the characteristic velocity, the unperturbed velocity at the infinity;
- $\tilde{L}_0 = \tilde{D}/\tilde{U}_\infty$ is the characteristic length;
- $\tilde{\Phi}_0 = \tilde{E}_\infty \tilde{L}_0 = \tilde{E}_\infty \tilde{D}/\tilde{U}_\infty$ is the characteristic potential;
- $\tilde{c}_0 = \tilde{c}_\infty = \tilde{K}_\infty/2$ is the characteristic ion concentration, the background neutral ion concentration.

It is convenient to take the dimensionless salt concentration in the following form:

$$K = \frac{\tilde{K}}{\tilde{c}_\infty} - 2 \tag{6}$$

so that $K \to 0$ far from the origin.

Equations (1)–(3) are expanded as follows:[1]

$$\frac{\partial K}{\partial t} + U\frac{\partial K}{\partial x} + V\frac{\partial K}{\partial y} = \frac{\partial^2 K}{\partial x^2} + \frac{\partial^2 K}{\partial y^2} + Q\,\delta(x)\,\delta(y), \tag{7}$$

$$\frac{\partial}{\partial x}\left[(K+2)\frac{\partial \Phi}{\partial x}\right] + \frac{\partial}{\partial y}\left[(K+2)\frac{\partial \Phi}{\partial y}\right] = 0, \tag{8}$$

$$\mathrm{Re}\left(\frac{\partial U}{\partial t} + U\frac{\partial U}{\partial x} + V\frac{\partial U}{\partial y}\right) + \frac{\partial \Pi}{\partial x} - \frac{\partial^2 U}{\partial x^2} - \frac{\partial^2 U}{\partial y^2} = \Lambda\left(\frac{\partial^2 \Phi}{\partial x^2} + \frac{\partial^2 \Phi}{\partial y^2}\right)\frac{\partial \Phi}{\partial x},$$

$$\mathrm{Re}\left(\frac{\partial V}{\partial t} + U\frac{\partial V}{\partial x} + V\frac{\partial V}{\partial y}\right) + \frac{\partial \Pi}{\partial y} - \frac{\partial^2 V}{\partial x^2} - \frac{\partial^2 V}{\partial y^2} = \Lambda\left(\frac{\partial^2 \Phi}{\partial x^2} + \frac{\partial^2 \Phi}{\partial y^2}\right)\frac{\partial \Phi}{\partial y}, \tag{9}$$

$$\frac{\partial U}{\partial x} + \frac{\partial V}{\partial y} = 0. \tag{10}$$

The boundary conditions (BCs) (4) in the dimensionless form are as follows:

$$x^2 + y^2 \to \infty: \quad U \to 1, \quad V \to 0, \quad K \to 0, \quad \frac{\partial \Phi}{\partial x} \to -1. \tag{11}$$

In the dimensionless equations above, $\mathrm{Re} = \frac{\tilde{\rho}\tilde{U}_\infty \tilde{L}_0}{\tilde{\mu}} = \frac{\tilde{\rho}\tilde{D}}{\tilde{\mu}}$ is the Reynolds number. For the aqueous NaCl solutions, Re $\sim 10^{-3}$. It is kept constant during our calculations. Thus, the problem is characterized by two dimensionless parameters

$$\Lambda = \frac{\tilde{\varepsilon}\tilde{D}\tilde{E}_\infty^2}{\tilde{\mu}\tilde{U}_\infty^2} \tag{12}$$

and

$$Q = \frac{\tilde{Q}}{\tilde{b}\tilde{c}_\infty \tilde{D}}. \tag{13}$$

Λ characterizes the strength of the electric field; Q is the dimensionless molar salt concentration flow rate.

The typical bulk concentration of the aqueous electrolytes varies in the range $\tilde{c}_\infty = 1 \div 10^3\,\mathrm{mol/m^3}$; the electric field is about $\tilde{E}_\infty = 0.5 \div 10\,\mathrm{kV/m}$; the diffusivity is $\tilde{D} = 10^{-9}\mathrm{m^2/s}$; the dynamic viscosity is $\tilde{\mu} = 1.1 \times 10^{-3}\,\mathrm{kg/(m\,s)}$; the electric permittivity for water is $\tilde{\varepsilon} = 7.0 \times 10^{-10}\,\mathrm{C^2\,s^2/(kg\,m^3)}$; the characteristic velocity in microfluidic devices $\tilde{U}_\infty$ is of the order of $10^{-2}\mathrm{cm/s}$. These ranges give us $\Lambda = 0.015 \div 5.0$.

III. OVERVIEW OF THE JET INSTABILITY THROUGH SOME NUMERICAL EXPERIMENTS

The system (7)–(10) was solved by direct numerical simulation (DNS) using the method developed in works;[4,5] therefore, we omit all the details of the method in the present work. During the calculations, the salt flux from the source was disturbed by imposing a small-amplitude broadband random noise, $Q(t) = \langle Q\rangle + \hat{Q}(t)$, which was convected downstream. Any disturbances to other quantities are caused by the small noise $\hat{Q}$, and they share its spectrum until nonlinear effects are strong enough. For the sake of simplicity, we will further use the symbol Q for the time-average flux $\langle Q\rangle$ in the discussion of DNS results. The goal is to study the stability of the jet flow through its spectrum downstream.

The calculations in Fig. 3 are presented for the typical unstable parameters, $\Lambda = 0.1$, and three values of Q, $Q = 2000$, 2500, and 2700 (see the explanation in the next paragraph and in the linear stability analysis). The snapshots of the concentration $K(x, y)$ are given for different time instants t. The first case does not fully show the instability features, and the last two are strongly unstable. At the initial time, the electrostatic field and the hydrodynamic flow are uniform for the whole space, $\Phi + x = 0$ and $U - 1 = 0$. The salt concentration everywhere is equal to the background concentration, $K = 0$ (in the dimensional form $\tilde{K} = 2\tilde{c}_\infty$). The source in the origin $x = y = 0$ emits additional salt to the liquid with the rate Q; this salt is convected to the right and diffuses at the same time. At small time, $t = 32$, all the additional salt is concentrated near the origin as a spot elongated in the x-direction. At larger time, $t = 232$, the advection prevails over the diffusion and the spot stretches significantly in the x-direction. At $t = 800$, we get a well-developed jet of concentration. The distortion of the velocity field by the Coulomb force is small and, thus, cannot be seen in the figure at this time (the explanation of this fact will be given later, in the study of the self-similar solution). At $t = 858$, we can notice a weak manifestation of instability in all three cases. This instability is

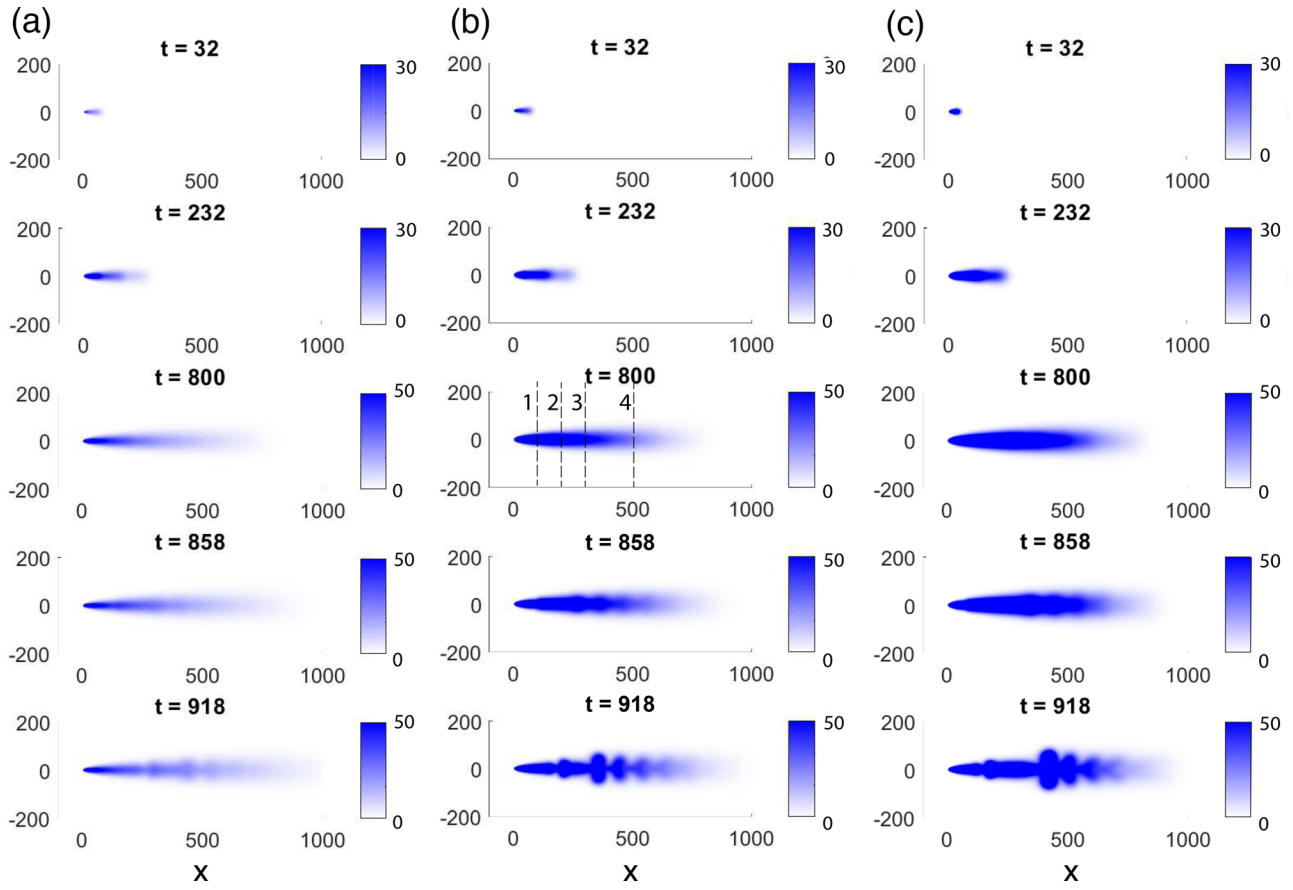

FIG. 3. Fields of $K(x, y, t)$ for $\Lambda = 0.1$: (a) $Q = 2000$, (b) $Q = 2500$ and (c) $Q = 2700$ at different time instants. (a) is an intermediate regime, (b) and (c) are unstable ones. The dashed lines at $t = 800$ (b) show the cross sections described later. 1: $x = 100$; 2: $x = 200$; 3: $x = 300$; 4: $x = 500$.

getting stronger, and at longer times, it becomes well-pronounced. This instability is of a convective nature,[37–40] the perturbations are carried to the right at approximately the speed of the external flow. The snapshots of the concentration with a pronounced instability are shown in Fig. 4 (Multimedia view).

There were certain difficulties to specify the exact threshold of instability. For a fixed Λ, there are two characteristic critical values of Q. For the higher one, the flow is always strongly unstable, but for the lower value of Q, the flow, sometimes, manifests a weak instability, and sometimes, it is stable: the outcome depends on the realization of the random initial conditions at the source. We will refer to such regimes as to "intermediate" ones.

IV. QUASI-ONE-DIMENSIONAL SOLUTIONS AND THEIR LINEAR STABILITY

In order to understand the physical nature of the above-mentioned instability, we fulfill a simplified analytical analysis of the problem. Let us first assume that the jet is steady, well-developed, and the electric potential and velocities are perturbed weakly with respect to their background values: $\tilde{\Phi} = -\tilde{E}_\infty \tilde{x} + \tilde{\varphi}$, $\tilde{U} = \tilde{U}_\infty + \tilde{u}$, $\tilde{V} = \tilde{v}$, $\max(\tilde{u}, \tilde{v}) \ll \tilde{U}_\infty$. Next, we assume that the longitudinal changes are slower than the transverse ones, $\partial/\partial\tilde{x} \ll \partial/\partial\tilde{y}$. We also consider the Stokes approximation of the creeping flow. The validation of these assumptions will be given *a posteriori*. In order to understand the orders of physical quantities and their relationships, the equations will be taken here in the dimensional form and will be gradually transformed to a convenient dimensionless form. Equation (1) along with BCs (4) turn into the following:

$$\tilde{U}_\infty \frac{\partial \tilde{K}}{\partial \tilde{x}} = \tilde{D} \frac{\partial^2 \tilde{K}}{\partial \tilde{y}^2}, \quad \tilde{K}\big|_{\tilde{y}\to\pm\infty} - 2\tilde{c}_\infty \to 0. \tag{14}$$

In the case of the classical free jet flow, a reference velocity is defined through the jet momentum.[41] Our case is different: the reference salt flux must be employed. If we define the salt flux in the $\tilde{x}$-direction for the line source of length $\tilde{b}$ as

$$\tilde{Q} = \tilde{b} \int_{-\infty}^{+\infty} \left(\tilde{K} - 2\tilde{c}_\infty\right) \tilde{U}_\infty \, d\tilde{y}, \tag{15}$$

it will coincide with the one determined by relation (2), i.e., $\tilde{Q} = \tilde{b} \int\int \tilde{q} \, d\tilde{x} d\tilde{y}$, thus $\tilde{Q}$ plays the same role as the classical jet momentum. This relation also selects a single solution from the family of solutions to the boundary-value problem (14).

Integrating (14) with respect to y yields

$$\tilde{U}_\infty \frac{\partial}{\partial \tilde{x}} \int_{-\infty}^{+\infty} \left(\tilde{K} - 2\tilde{c}_\infty\right) d\tilde{y} = \tilde{D} \frac{\partial\left(\tilde{K} - 2\tilde{c}_\infty\right)}{\partial \tilde{y}}\bigg|_{-\infty}^{+\infty} = 0,$$

i.e., $\tilde{Q}$ does not depend on $\tilde{x}$. In Eq. (15), $\tilde{b}$ is the characteristic size in the $\tilde{z}$-direction (in a 2D calculation, it can be taken as unity or as the real size for comparison with experiments), see Fig. 2. Formally, Eq. (15) is easy to get by integration of Eq. (14) from $\tilde{y} = -\infty$ to $+\infty$.

Equation (15) yields

$$\tilde{Q} = \tilde{b}\, \tilde{c}_\infty \tilde{U}_\infty \int_{-\infty}^{+\infty} K d\tilde{y} \quad \text{with } K = \tilde{K}/\tilde{c}_\infty - 2. \tag{16}$$

In order to solve Eq. (14), we introduce the classical self-similar variable:

$$\eta = \frac{\tilde{y}}{\tilde{\delta}} = \tilde{y}\sqrt{\frac{\tilde{U}_\infty}{\tilde{D}\tilde{x}}} = \frac{y}{\sqrt{x}} \quad \text{with } x = \frac{\tilde{x}}{\tilde{L}_0}, \; y = \frac{\tilde{y}}{\tilde{L}_0}, \; \tilde{L}_0 = \frac{\tilde{D}}{\tilde{U}_\infty}, \tag{17}$$

where $\tilde{\delta} = \sqrt{\tilde{D}\tilde{x}/\tilde{U}_\infty}$ is the electric boundary layer thickness. Then, Eq. (16) turns into the following one:

$$\tilde{Q} = \tilde{b}\, \tilde{c}_\infty \tilde{D}\sqrt{x} \int_{-\infty}^{+\infty} K d\eta. \tag{18}$$

In order for $\tilde{Q}$ to remain constant with respect to x, we must assume that K is inversely proportional to $\sqrt{x}$:

$$K = \frac{Q}{2\sqrt{\pi x}}\, k(\eta), \tag{19}$$

where Q is determined by Eq. (13) and $k(\eta)$ is the solution of the transformed boundary-value problem (14):

$$k'' + \frac{1}{2}(\eta k)' = 0, \quad k'|_{\eta=0} = 0, \quad k|_{\eta\to\pm\infty} \to 0. \tag{20}$$

The solution to (20) is $k = \exp(-\eta^2/4)$, so

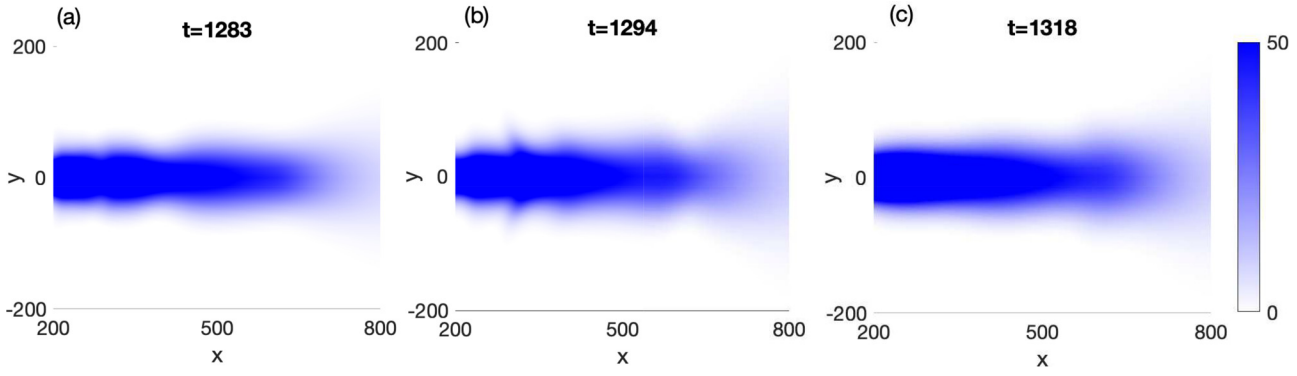

FIG. 4. Fields of $K(x, y, t)$ for $\Lambda = 0.1$ and $Q = 2700$ at different time instants. (a) t = 1283, (b) t = 1294, and (c) t = 1318. Multimedia view: https://doi.org/10.1063/5.0098652.1.

$$K = \frac{Q}{2\sqrt{\pi x}}\, e^{-\frac{\eta^2}{4}} = \frac{Q}{2\sqrt{\pi x}} \exp\left(-\frac{y^2}{4x}\right),$$
$$\tilde{K} = 2\,\tilde{c}_\infty \left(\frac{Q}{4\sqrt{\pi x}} e^{\frac{-y^2}{4x}} + 1\right). \tag{21}$$

The advection and diffusion of the concentration $\tilde{K}$ disturb the initial concentration, and thus, they also disturb the electric conductivity $\tilde{\sigma}$, which is linearly proportional to the concentration:

$$\tilde{\sigma} = \frac{\tilde{F}^2 \tilde{D}}{\tilde{R}\tilde{T}}\,\tilde{K}$$

(see Ref. 35). Here, $\tilde{F}$ is the Faraday constant, $\tilde{R}$ is the universal gas constant, and $\tilde{T}$ is the absolute temperature. In turn, according to the second part of Eq. (1), the perturbation of the conductivity causes the distortion of the electric field:

$$\frac{\partial}{\partial \tilde{y}}\left(\tilde{K}\,\frac{\partial \tilde{\Phi}}{\partial \tilde{y}}\right) = -\frac{\partial}{\partial \tilde{x}}\left(\tilde{K}\,\frac{\partial \tilde{\Phi}}{\partial \tilde{x}}\right) \approx \tilde{E}_\infty \frac{\partial \tilde{K}}{\partial \tilde{x}} = \frac{\tilde{D}\tilde{E}_\infty}{\tilde{U}_\infty}\frac{\partial^2 \tilde{K}}{\partial \tilde{y}^2}. \tag{22}$$

Here, we have substituted the right-hand side of Eq. (14) and have kept only the leading-order terms. We can treat (22) as a second-order ordinary differential equation (ODE) on Φ:

$$\frac{d}{d\tilde{y}}\left(\tilde{K}\,\frac{d\tilde{\Phi}}{d\tilde{y}}\right) = \frac{\tilde{D}\tilde{E}_\infty}{\tilde{U}_\infty}\frac{d^2 \tilde{K}}{d\tilde{y}^2}$$

and solve it by two successive integrations with respect to y. Since $d\tilde{\Phi}/d\tilde{y} \to 0$, $d\tilde{K}/d\tilde{y} \to 0$ as $\tilde{y} \to \pm\infty$, we can write the solution for $\tilde{\Phi}$ as follows:

$$\tilde{\Phi} = -\tilde{E}_\infty \tilde{x} + \frac{\tilde{D}\tilde{E}_\infty}{\tilde{U}_\infty} \ln\left[\frac{Q}{4\sqrt{\pi x}} \exp\left(-\frac{y^2}{4x}\right) + 1\right]. \tag{23}$$

Here, we set the zero-potential level at $\tilde{x} = 0$, $\tilde{y} \to \infty$. By taking the characteristic potential as $\tilde{\Phi}_0 = \tilde{E}_\infty \tilde{D}/\tilde{U}_\infty = \tilde{E}_\infty \tilde{L}_0$, the corresponding dimensionless form can be written as

$$\Phi = -x + \ln\left[\frac{Q}{4\sqrt{\pi x}} \exp\left(-\frac{y^2}{4x}\right) + 1\right],$$
$$\frac{\partial \Phi}{\partial x} = -1 + \frac{(y^2 - 2x)\, Q \exp\left(-\frac{y^2}{4x}\right)}{4x^2\left[Q \exp\left(-\frac{y^2}{4x}\right) + 4\sqrt{\pi x}\right]}. \tag{24}$$

We assume that the inertial terms for microfluidic flows are negligibly small and, as it was mentioned earlier, $\partial/\partial\tilde{x} \ll \partial/\partial\tilde{y}$. Then, Eq. (3) leads to

$$\frac{\partial \tilde{\Pi}}{\partial \tilde{x}} + \tilde{\mu}\frac{\partial^2 \tilde{U}}{\partial \tilde{y}^2} = \tilde{\varepsilon}\frac{\partial^2 \tilde{\Phi}}{\partial \tilde{y}^2}\tilde{E}_\infty, \quad \frac{\partial \tilde{\Pi}}{\partial \tilde{y}} = \tilde{\varepsilon}\frac{\partial^2 \tilde{\Phi}}{\partial \tilde{y}^2}\frac{\partial \tilde{\Phi}}{\partial \tilde{y}}. \tag{25}$$

Direct integration of the second equation of (25) yields $\tilde{\Pi} = \frac{\tilde{\varepsilon}}{2}(\partial\tilde{\Phi}/\partial\tilde{y})^2 + \tilde{f}(\tilde{x})$, where the unknown function $\tilde{f}(\tilde{x})$ is determined from the condition that the pressure $\tilde{\Pi}$ is the same everywhere in the flow field outside of the boundary layer. Our boundary conditions lead to $\tilde{f} \equiv 0$. Thus, (25) turns into the following equation:

$$\tilde{\mu}\frac{\partial^2 \tilde{U}}{\partial \tilde{y}^2} = \tilde{\varepsilon}\frac{\partial^2 \tilde{\Phi}}{\partial \tilde{y}^2}\tilde{E}_\infty - \tilde{\varepsilon}\frac{\partial^2 \tilde{\Phi}}{\partial \tilde{x}\partial \tilde{y}}\frac{\partial \tilde{\Phi}}{\partial \tilde{y}}. \tag{26}$$

The second term in the right-hand side of Eq. (26) has order of $\underline{O}(1/x^4)$ as $x \gg 1$, which is small in comparison with the first term, $\underline{O}(1/x^{3/2})$, so the former one can be neglected. Knowing that $\partial\tilde{U}/\partial\tilde{y} \to 0$, $\partial\tilde{\Phi}/\partial\tilde{y} \to 0$ and $\tilde{U} \to \tilde{U}_\infty$ at $\tilde{y} \to \pm\infty$, the solution of simplified Eq. (26) can be found by double integration with respect to $\tilde{y}$ and using the corresponding BCs:

$$\tilde{U} = \tilde{U}_\infty + \frac{\tilde{\varepsilon}\tilde{D}\tilde{E}_\infty^2}{\tilde{\mu}\tilde{U}_\infty} \ln\left[\frac{Q}{4\sqrt{\pi x}} \exp\left(-\frac{y^2}{4x}\right) + 1\right] \tag{27}$$

or in the dimensionless form

$$U = 1 + \Lambda \ln\left[\frac{Q}{4\sqrt{\pi x}} \exp\left(-\frac{y^2}{4x}\right) + 1\right], \tag{28}$$

where Λ is defined by Eq. (12).

For the classical 2D jet, the boundary layer thickness is proportional to $x^{2/3}$,[41] while in the present case, it is proportional to $x^{1/2}$. For the classical free jet, $U \sim 1/x^{1/3}$,[41] and for this jet, the dependence of U on x is more tricky. Our case also reminds a wake behind bodies, where $\eta = y/\sqrt{x}$.

Our analytical solution has some restrictions. In order to get this solution, we have assumed the following.

(a) The self-similar solution (21) for the salt concentration is valid if we are far enough from the source. The difference between the exact numerical solution and the self-similar one decreases with increasing of x as $\underline{O}(1/x)$. This evaluation is easily done by calculating the skipped terms in Eq. (14).
(b) The difference between the electric field disturbed by the jet and the main field $\tilde{E}_\infty$ is of the order of $1/\sqrt{x}$, see Eq. (24).
(c) According to Eq. (28), the velocity field differs from the undisturbed one proportionally to Λ; thus, at $\Lambda \ll 1$, the analytical analysis provides a good approximation.
(d) The Navier–Stokes system is taken in the Stokes approximation, and therefore, the properly defined Reynolds number must be small, $\tilde{\delta}\tilde{\rho}\tilde{U}_\infty/\tilde{\mu} \ll 1$. Substituting $\tilde{\delta} = \sqrt{\tilde{D}\tilde{x}/\tilde{U}_\infty}$ and using dimensionless x result in $Re_\delta = (\tilde{\rho}\tilde{D}/\tilde{\mu})\sqrt{x} = \sqrt{x}/Sc$. Here, $Sc = \frac{\tilde{\mu}}{\tilde{\rho}\tilde{D}}$ is the Schmidt number, which, in our case, is about 1100, and hence, x must be of the order much less than about 10^6.
(e) For a jet of salt extended in the x-direction to be formed, it is necessary for the Péclet number $Pe_\delta = \tilde{\delta}\tilde{U}_\infty/\tilde{D}$ based on $\tilde{\delta}$ to be large. This condition provides $Pe_\delta = \sqrt{x} \gg 1$.

The dependencies of Reynolds and Péclet numbers on x are given in Table I. The instability manifests itself at the distances from $x = 50$ to $x = 1000$ (see typical results in Fig. 3), where all the requirements are met.

The comparison between these analytical self-similar solutions and the results of DNS is presented in Fig. 5. The numerical results are depicted, on the one hand, at the time when the jet is well-developed, but, on the other hand, at the time when the manifestation of instability is negligible. We found $Q = 2500$ and $t = 800$ suitable for this purpose. The snapshots 1, 2, 3, and 4 correspond to the respective

TABLE I. Typical values of Reynolds and Péclet numbers based on the boundary layer thickness at different dimensionless distances.

x	5	10	50	100	200	300	500	1000
Re_δ (must be $\ll 1$)	0.002	0.003	0.006	0.009	0.013	0.015	0.020	0.029
Pe_δ (must be $\gg 1$)	2.24	3.2	7.1	10.0	14.1	17.3	22.4	31.6

cross sections shown in Fig. 3(b). The profiles of (a) concentration, (b) electric potential, and (c) the x-component of velocity are plotted for these cross sections. In the cross sections 1, 2, and 3, all analytical profiles match our DNS very well. Cross section 4 is located near the moving front of the jet, so the assumptions for the self-similar solution are no longer satisfied. Therefore, it is not surprising that, in the last cross section, there is no coincidence of the analytical solution with the numerical one.

V. LINEAR STABILITY OF SELF-SIMILAR SOLUTIONS

The study of linear stability of self-similar flows is an important part of our analysis and a good addition to the direct numerical simulation since it allows not only to confirm or refine the results of the DNS but also to clarify some important details that cannot be obtained from the DNS. The usual procedure for the theory of hydrodynamic instability is to look for a solution in the form

$$f = f_0(y) + \hat{f}(y)e^{\theta}, \quad \theta = i(\alpha x - \omega t) = i(\alpha x - \alpha c t), \tag{29}$$

where $f_0(y)$ is the one-dimensional solution describing the unperturbed flow, and the perturbation is taken in the form of the elementary sinusoidal solution. The subscript 0 is related to the mean solution, the hat, to the perturbations. Here, $\hat{f}(y)$ is the eigenfunction, α is the wavenumber of the perturbation, $\omega = \alpha c$ is the frequency, and c is the phase velocity of the wave.

The self-similar solution (21), unlike f_0 in (29), is slowly changing in the x-direction. Such non-parallel flows are not exceptional in the theory of stability; rather, strictly parallel flows, such as Poiseuille or Couette flow, are the exceptions to the rule.[42,43] The flow in a Blasius boundary layer, flows in free jets, wakes behind a body and many

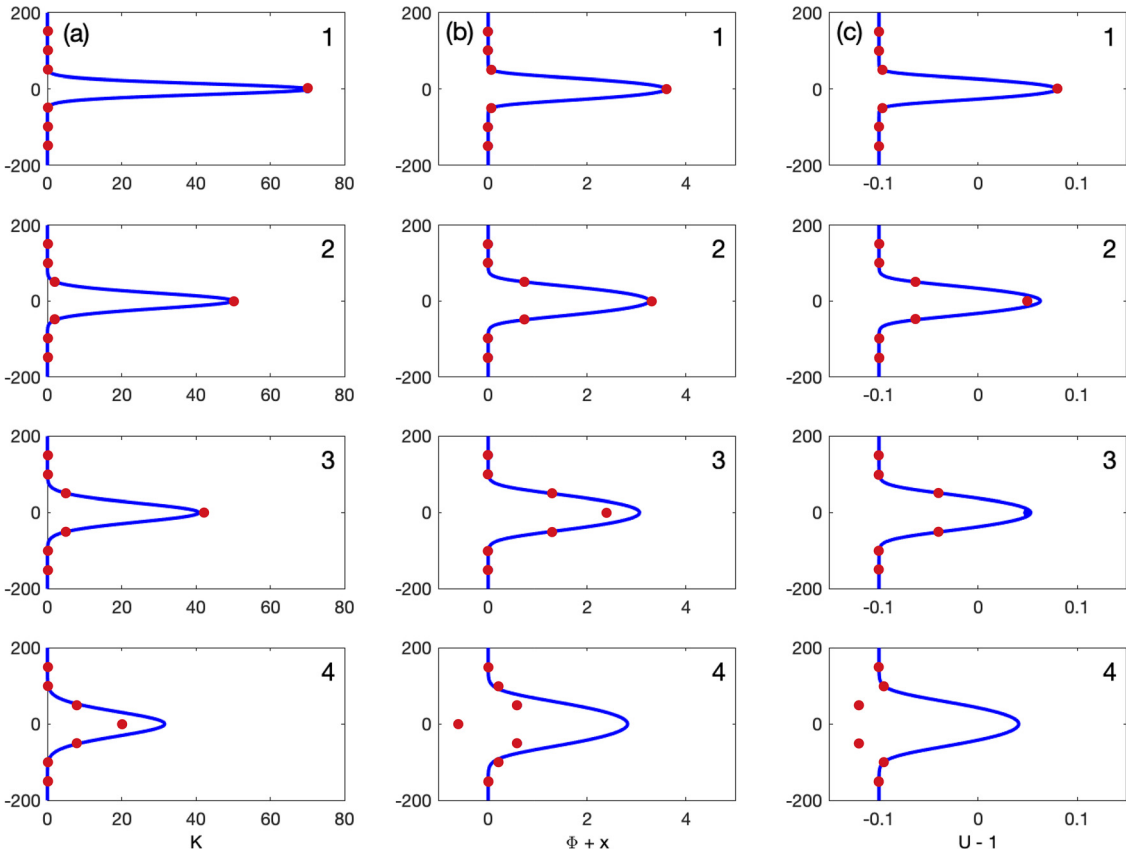

FIG. 5. The profiles of (a) concentration K, (b) electric potential $\Phi + x$ and (c) velocity U–1 for the cross sections 1, 2, 3, and 4 in Fig. 3(b). Solid line stands for the analytical solution, markers •, for the DNS. $Q = 2500$, $\Lambda = 0.1$ and $t = 800$.

others are not parallel flows; however, the study of their linear stability under the assumption that they are locally parallel usually leads to fairly good results. Thus, we seek a solution to the stability problem in the form similar to (29) for all the unknowns, $f = \{K, \Phi, \Pi, \mathbf{U}\}$, assuming that the variation in the longitudinal direction is much slower than in the normal one. In the linear stability analysis, we neglect the inertial terms, assuming $\mathrm{Re} = 0$.

Upon substitution of (29) for all the unknowns into Eqs. (7)–(10) and BCs (11), linearization of the equations with respect to the perturbations, and omitting the subscript 0 in the mean solution, we get the system of equations

$$-i\omega\hat{K} + i\alpha U\hat{K} + V\hat{K}' + K'\hat{V} = \hat{K}'' - \alpha^2\hat{K}, \tag{30}$$

$$(K+2)\hat{\Phi}'' + K'\hat{\Phi}' + \Phi''\hat{K} + \Phi'\hat{K}' + i\alpha A_1\hat{K} - \alpha^2(K+2)\hat{\Phi} = 0, \tag{31}$$

$$-i\alpha\hat{\Pi} + \hat{U}'' - \alpha^2\hat{U} = \Lambda\left[-i\alpha\Phi''\hat{\Phi} - A_1\left(\hat{\Phi}'' - \alpha^2\hat{\Phi}\right)\right], \tag{32}$$

$$-\hat{\Pi}' + \hat{V}'' - \alpha^2\hat{V} = -\Lambda\left[\Phi''\hat{\Phi}' + \Phi'\left(\hat{\Phi}'' - \alpha^2\hat{\Phi}\right)\right], \tag{33}$$

$$i\alpha\hat{U} + \hat{V}' = 0, \tag{34}$$

where the prime means the derivative with respect to y. Here

$$A_1 = -1 + \frac{Q\exp\left(-\frac{y^2}{4x}\right)(y^2 - 2x)}{4x^2\left[Q\exp\left(-\frac{y^2}{4x}\right) + 4\sqrt{\pi x}\right]}, \qquad V = -\int_0^y \frac{\partial U}{\partial x}\,dy.$$

The BCs far from the jet are as follows:

$$y \to \pm\infty: \quad \hat{U} \to 0, \quad \hat{V} \to 0, \quad \hat{K} \to 0, \quad \hat{\Phi} \to 0. \tag{35}$$

In the center of the jet, $A_1 + 1 = \underline{O}(1/x)$, and far from the center, $A_1 + 1$ is exponentially small with respect to x.

Equations (30)–(35) constitute an eigenvalue problem, but the final formulation of this problem allows two possibilities. Let us first decompose α and ω into real and imaginary parts:

$$\theta = i((\alpha_r + i\alpha_i)x - (\omega_r + i\omega_i)t) = (-\alpha_i x + \omega_i t) + i(\alpha_r x - \omega_r t). \tag{36}$$

Similarly, $c = c_r + ic_i$. In a temporal stability analysis, we constrain α to be a real number, $\alpha = \alpha_r$, $\alpha_i = 0$. This means that we consider only waves that do not grow in the streamwise direction. They can grow or decay in time, depending on the sign of $\omega_i = \alpha c_i$. At $\alpha c_i > 0$, the perturbations grow in time, and at $\alpha c_i < 0$, they decay. In this case, α is a given real number and ω is a complex eigenvalue.

In a spatial stability analysis, we constrain ω to be a real number instead, $\omega_i = 0$. This means that we force sinusoidality at a particular point in space and see whether the perturbations grow ($\alpha_i < 0$) or decay ($\alpha_i > 0$) downstream. This possibility assumes that the frequency ω is a given real number and α is a complex eigenvalue.

Technically, the solution of the temporal stability eigenvalue problem is much easier than the solution of the spatial problem. On the other hand, in our open flow problem, the disturbances grow downstream and it would be correct to use the spatial stability formulation. Fortunately, at small and moderate growth rates, we can perform the calculations for the temporal problem and then recalculate the results to the spatial formulation using the famous Gaster's theorem.[44] When solving the temporal stability problem, we obtain the real part of ω, $\omega_r = \alpha c_r$, and the temporal growth rate $\omega_i = \alpha c_i$. Hence, we determine the phase velocity, $c_r = \omega_r/\alpha$, $c_i = \omega_i/\alpha$, and their group velocity, $v_g = \partial\omega_r/\partial\alpha$. We can, thus, rewrite (36) as follows:

$$\theta = (-\alpha_i + i\alpha_r)x - i\omega_r t = \left(-\alpha_i + i\frac{\omega_r}{c_r}\right)x - i\omega_r t.$$

According to Ref. 44, the spatial problem is connected to the temporal one through the following relation:

$$v_g \simeq -\frac{\omega_i}{\alpha_i}, \tag{37}$$

where v_g can be taken from any problem statement. In our case, α_i for the spatial problem can be calculated from the values of ω_i and v_g from the temporal problem. Then, the spatial stability problem can be expressed with the following simple relation:

$$\theta = \left(\frac{\omega_i}{v_g} + i\frac{\omega_r}{c_r}\right)x - i\omega_r t,$$

where all the quantities are taken from the temporal formulation.

We, thus, consider Eqs. (30)–(35) to be an eigenvalue problem for the complex ω with a fixed α. Upon solving this problem, we obtain triplets (α, c_r, c_i). Having these, we are able to compute ω_r and ω_i and, eventually, recalculate the results to the spatial evolution according to the Gaster's transformation Eq. (37). If $\alpha_i > 0$ for all frequencies ω_r, the self-similar jet solution is stable; if $\alpha_i < 0$ for any frequency, it is unstable.

The discretization was realized by expanding the unknown functions in the Hermite series. The eigenvalues were calculated by the QR-algorithm. Only the most dangerous eigenvalue (with the largest growth rate) was taken from the discrete spectrum. The eigenvalue problem was solved for as many values of α as needed to provide a smooth enough grid with respect to ω_r. The solutions now depend on three parameters: Q, Λ, and, additionally, x_0. The latter parameter means a cross section in x where the mean solution is taken.

The fact that our jet flows lose their stability at zero Reynolds numbers is already a peculiar feature. The physical mechanism of the stability loss in the classical free jets and wakes behind bodies is associated with the inertial forces and can only occur at large Reynolds numbers. A necessary condition for such instability for the infinitely large Reynolds numbers is the presence of an inflection point on the velocity profile (the well-known Rayleigh theorem[42]). On the contrary, our instability occurs at the infinitely small Reynolds numbers, and we do not have such a simple and elegant physical explanation for it.

In Fig. 6(a), the dependence of the spatial growth rate α_i on the frequency ω_r, which is determined by Eq. (37) and characterizes downstream instability, is presented for the different cross sections x_0 and fixed Λ and Q. With increasing the distance from the source x_0, the flow becomes more stable, so the most unstable cross section is located just near the source $x_0 = 0$. Such feature is rather unusual for the classical free jets and wakes,[41–43] which remain unstable for far-away cross sections x_0. The phase velocity of the perturbation as a function of the frequency ω_r is presented in Fig. 6(b), and it shows that there is practically no wave dispersion. The disturbances can propagate a bit faster than the main flow or a bit slower, but, in any way, the difference does not exceed 5% of the main velocity.

To emphasize, there is a spatial interval $0 < x_0 < x_0^*$, where the flow is unstable. For $x_0 > x_0^*$, any perturbation decays. A typical dependence of x_0^* on the molar salt concentration flow rate at fixed Λ

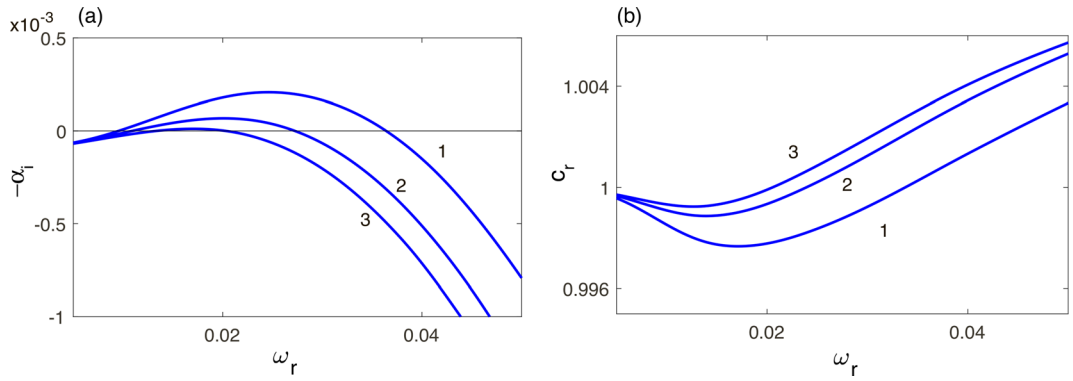

FIG. 6. (a) Spatial growth rate determined by Eq. (37) and (b) the phase velocity of perturbations vs the frequency ω_r for $\Lambda = 10^{-2}$, $Q = 1000$ and different x_0: 1: $x_0 = 50$, 2: $x_0 = 100$, 3: $x_0 = 150$.

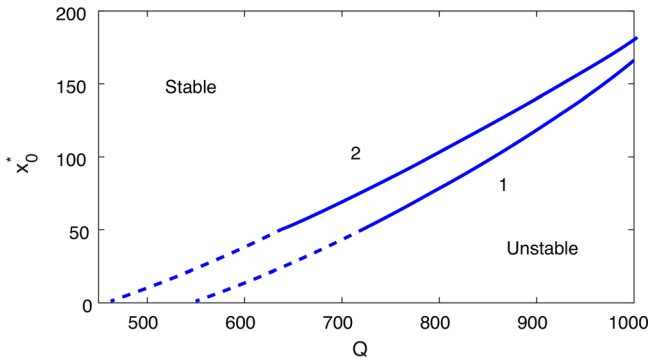

FIG. 7. The dependencies of the critical x_0^* on Q: 1—$\Lambda = 0.01$, 2—$\Lambda = 0.02$. The fractions of the curves from $x_0^* = 0$ till $x_0^* = 50$ violate our assumptions (see Table I) and are shown by dashed lines.

is shown in Fig. 7: the unstable interval $0 < x_0 < x_0^*$ expands with increasing of Q. The calculations were also performed for larger values of Λ, up to 0.1. With an increase in any of the parameters, Λ or Q, the unstable spatial interval expands.

The existence of the critical value x_0^* is due to the fact that the intensity of the salt concentration decreases downstream and the electrical forces are not strong enough to overcome the dissipation and cause the instability. According to the theory of linear stability, for $x > x_0^*$, the perturbations should decay rapidly, but when x_0^* is reached, the amplitude of the perturbations is already large enough so that they obey nonlinear laws. Numerical modeling shows that the formed nonlinear structures will only slowly diffuse further, practically without changing the amplitude.

It is instructive to compare the results of the linear analysis with the DNS, especially taking into account the fact that the linear stability analysis has an additional parameter, x_0. The length x_0 must be large enough to allow small random noise to evolve toward coherent structures of a finite amplitude.

First, we compare the frequencies of maximum spatial growth rate from the linear stability analysis, ω_r^*, with the characteristic frequencies of the DNS at the beginning of the instability (selected from the initial noise $\hat{Q}$), Fig. 8. There is a good fit between these two approaches, except for small Λ, where ω_r^* could not be determined exactly because the resulting period exceeded the simulation time.

After a transition period, the jet flow is established in the whole spatial interval (in our case, it is $0 < x < 1000$). The detailed spectrum

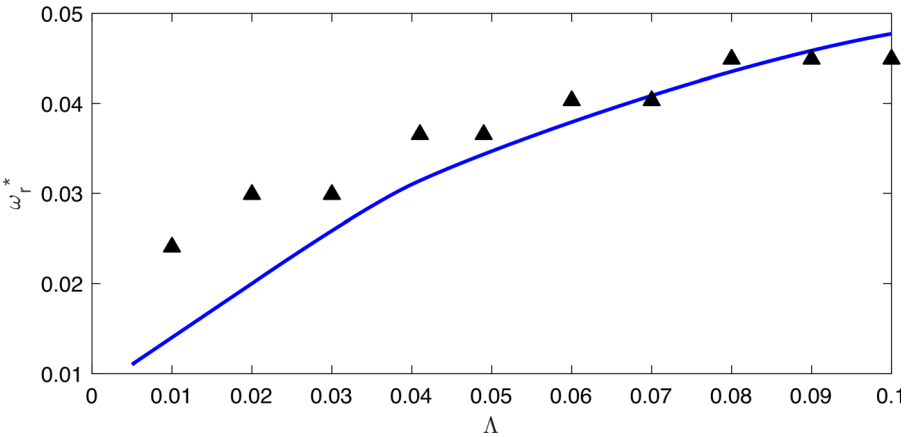

FIG. 8. The dependencies of the critical frequency ω_r^* on Λ. Solid line corresponds to the linear stability analysis and stands for $x_0 = 250$, and the triangles correspond to the DNS-obtained frequency of the most dangerous modes.

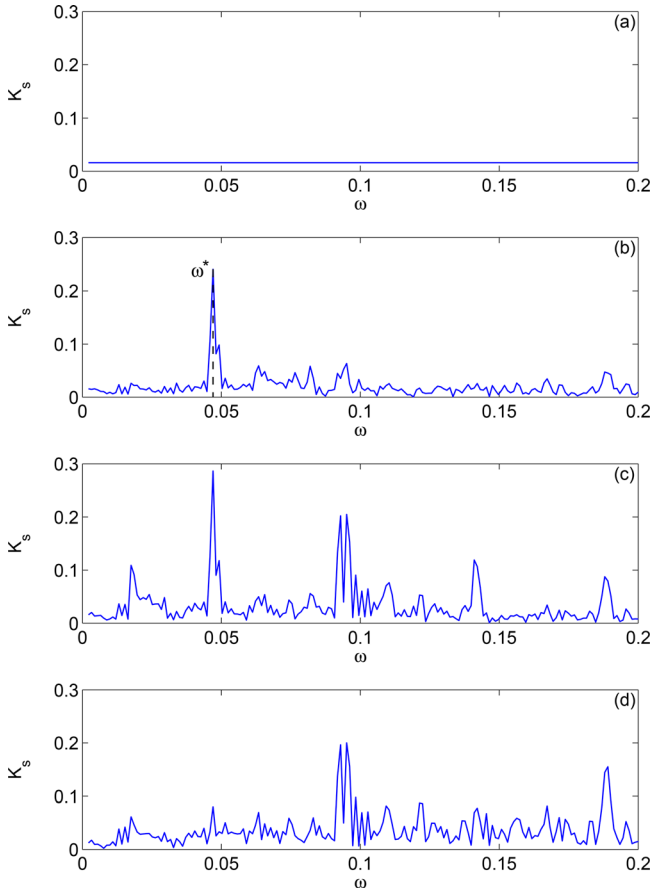

FIG. 9. Time spectrum $K_S(\omega) = |\int K(x = x_0, y = 0)e^{-2\pi i t\omega}dt|$ in different stations downstream: (a) $x_0 = 0$, (b) $x_0 = 50$, (c) $x_0 = 200$, and (d) $x_0 = 500$. $\Lambda = 0.1$ and average $Q = 2500$.

distribution at different stations downstream is presented in Fig. 9. To mimic a broadband white noise, the amplitudes of the spectrum were taken equal, but their phases were set by a random number generator in the interval of their periodicity. Thus, the initial spectrum is a constant with a given amplitude, which characterizes the level of the white noise $\hat{Q}$, Fig. 9(a). (The snapshots are taken with a small delay in t in order to see the effect of $\hat{Q}$ on K.) For small distances from the source, all the amplitudes grow according to the linear stability theory and the linear filtering mechanism singles out a narrow band of frequencies near the most dangerous one, $\omega^* \approx 0.05$, see Fig. 9(b). For larger times, the perturbations show typical nonlinear features: one can clearly see the overtones $2\,\omega^*$, $3\,\omega^*$, and subharmonic effects at small ω, Fig. 9(c). At the last station, shown in Fig. 9(d), the primary frequency ω^* decays practically to zero, but the overtones are visible. Thus, the typical size of the coherent structure in x-direction decreases by half. This effect can be clearly seen in Fig. 3(b), $t = 872$.

VI. CONCLUSIONS

We theoretically investigated a salt emitted from the point source into its background aquatic solution under the external electrostatic field. The electrohydrodynamic instability of this flow is a prototype for more complex microfluidic instabilities.[20–34] The solution is governed by two dimensionless parameters, the source flow rate Q and the electric field strength Λ. Unlike classical macrojets, this flow was considered in microscales and, therefore, at low Reynolds numbers, but at high Péclet numbers so that the salt advection prevails over the diffusion.

Numerical simulation of the complete nonlinear system of equations was carried out for various values of the parameters. The simulation showed that a salt spot of enhanced concentration appears at the initial moment of time near the source. This spot is convected downstream and spreads to the sides by diffusion, becoming more elongated and eventually forming a microjet. At sufficiently large times, the jet flow establishes over the entire computational domain. The spatial inhomogeneity of the salt concentration causes the inhomogeneity of the electrical conductivity and leads to the appearance of the Coulomb forces and, eventually, the electrohydrodynamic instability. The critical parameters were found when the flow becomes unstable. For the unstable case, a small-amplitude broadband random noise turns into a narrow band of frequencies by the linear instability filtering mechanism. This instability is of a convective nature, the unstable perturbations propagate downstream at approximately the speed of the external flow and turn into nonlinear coherent structures of larger frequencies. It was found that a twofold increase of Λ can enlarge the instability area by as much as 50% for moderate source flow rate ($Q = 700$, Fig. 7). At large flow rates ($Q = 1000$), a 10% increase can be achieved.

Along with the DNS, an analytical self-similar solution of a well-developed steady microjet was obtained. The boundary layer thickness is expanding downstream as $\sqrt{x}$. The profiles of salt concentration, electric potential, and velocity for the self-similar solution and for the DNS are in rather good correspondence. The obtained analytical solution was assumed to be locally parallel and was investigated for linear stability in the temporal formulation. Using Gaster's theorem, the results were recalculated into the spatial formulation. The critical values of parameters—the frequency ω_r^* and the maximum spatial growth rate frequencies—were in good quantitative agreement with the DNS: the mean error is about 8% (Fig. 8).

ACKNOWLEDGMENTS

The work was supported by the grant through the Russian Science Foundation, Project No. 22–29-00307. The research was carried out using the equipment of the shared research facilities of HPC computing resources at Lomonosov Moscow State University.

AUTHOR DECLARATIONS

Conflict of Interest

The authors have no conflicts to disclose.

Author Contributions

Sakir Amiroudine: Conceptualization (equal), Methodology (equal), Supervision (equal), and Writing – review and editing (equal). **Evgeny A. Demekhin:** Conceptualization (equal), Funding acquisition (equal), Investigation (equal), Methodology (equal), Writing – original draft (equal), and Writing – review and editing (equal). **Georgy S. Ganchenko:** Investigation (equal), Methodology (equal), Resources (equal), Software (equal), Visualization (equal), and Writing –

original draft (equal). **Vladimir S. Shelistov:** Data curation (equal), Investigation (equal), Software (equal), Validation (equal), Visualization (equal), and Writing – review and editing (equal). **Elizaveta Frants:** Data curation (equal), Software (equal), Validation (equal), and Visualization (equal).

DATA AVAILABILITY

The data that support the findings of this study are available from the corresponding author upon reasonable request.

REFERENCES

[1]H.-C. Chang, G. Yossifon, and E. A. Demekhin, "Nanoscale electrokinetics and microvortices: How microhydrodynamics affects nanofluidic ion flux," Annu. Rev. Fluid Mech. **44**, 401–426 (2012).

[2]I. Rubinstein and B. Zaltzman, "Electro-osmotically induced convection at a permselective membrane," Phys. Rev. E **62**, 2238–2251 (2000).

[3]B. Zaltzman and I. Rubinstein, "Electro-osmotic slip and electroconvective instability," J. Fluid Mech. **579**, 173–226 (2007).

[4]E. A. Demekhin, V. S. Shelistov, and S. V. Polyanskikh, "Linear and nonlinear evolution and diffusion layer selection in electrokinetic instability," Phys. Rev. E **84**, 036318 (2011).

[5]E. A. Demekhin, N. V. Nikitin, and V. S. Shelistov, "Three-dimensional coherent structures of electrokinetic instability," Phys. Rev. E **90**, 013031 (2014).

[6]V. S. Pham, Z. Li, K. M. Lim, J. K. White, and J. Han, "Direct numerical simulation of electroconvective instability and hysteretic current-voltage response of a permselective membrane," Phys. Rev. E **86**, 046310 (2012).

[7]C. L. Druzgalski, M. B. Andersen, and A. Mani, "Direct numerical simulation of electroconvective instability and hydrodynamic chaos near an ion-selective surface," Phys. Fluids **25**, 110804 (2013).

[8]A. Mani and K. M. Wang, "Electroconvection near electrochemical interfaces: Experiments, modeling, and computation," Annu. Rev. Fluid Mech. **52**, 509–529 (2020).

[9]S. M. Rubinstein, G. Manukyan, A. Staicu, I. Rubinstein, B. Zaltzman, R. G. H. Lammertink, F. Mugele, and M. Wessling, "Direct observation of nonequilibrium electroosmotic instability," Phys. Rev. Lett. **101**, 236101 (2008).

[10]G. Yossifon and H.-C. Chang, "Selection of nonequilibrium overlimiting currents: Universal depletion layer formation dynamics and vortex instability," Phys. Rev. Lett. **101**, 254501 (2008).

[11]S. J. Kim, Y.-C. Wang, J. H. Lee, H. Jang, and J. Han, "Concentration polarization and nonlinear electrokinetic flow near a nanofluidic channel," Phys. Rev. Lett. **99**, 044501 (2007).

[12]V. V. Nikonenko, N. D. Pismenskaya, E. I. Belova, P. Sistat, P. Huguet, G. Pourcelly, and C. Larchet, "Intensive current transfer in membrane systems: Modelling, mechanisms and application in electrodialysis," Adv. Colloid Interface Sci. **160**, 101–123 (2010).

[13]E. N. Kalaydin, N. Y. Ganchenko, G. S. Ganchenko, N. V. Nikitin, and E. A. Demekhin, "Thermoelectrokinetic instability and salt superconcentration near permselective electric membranes," Phys. Rev. Fluids **2**, 114201 (2017).

[14]E. A. Demekhin, S. Amiroudine, G. S. Ganchenko, and N. Y. Khasmatulina, "Thermoelectroconvection near charge-selective surfaces," Phys. Rev. E **91**, 063006 (2015).

[15]P. Kumar, S. M. Rubinstein, I. Rubinstein, and B. Zaltzman, "Mechanisms of hydrodynamic instability in concentration polarization," Phys. Rev. Res. **2**, 033365 (2020).

[16]M. Sheikholeslami and Z. Ebrahimpour, "Thermal improvement of linear Fresnel solar system utilizing Al_2O_3-water nanofluid and multi-way twisted tape," Int. J. Therm. Sci. **176**, 107505 (2022).

[17]M. Sheikholeslami, Z. Said, and M. Jafaryar, "Hydrothermal analysis for a parabolic solar unit with wavy absorber pipe and nanofluid," Renewable Energy **188**, 922–932 (2022).

[18]M. Sheikholeslami, M. Jafaryar, M. B. Gerdoodbary, and A. H. Alavi, "Influence of novel turbulator on efficiency of solar collector system," Environ. Technol. Innovation **26**, 102383 (2022).

[19]M. Sheikholeslami and S. A. Farshad, "Nanoparticles transportation with turbulent regime through a solar collector with helical tapes," Adv. Powder Technol. **33**, 103510 (2022).

[20]J. F. Hoburg and J. R. Melcher, "Electrohydrodynamic mixing and instability induced by co-linear fields and conductivity gradients," Phys. Fluids **20**, 903–911 (1977).

[21]J. R. Melcher and G. I. Taylor, "Electrohydrodynamics: A review of the role of interfacial shear stresses," Annu. Rev. Fluid Mech. **1**, 111–146 (1969).

[22]J. R. Melcher, *Continuum Electromechanics* (The MIT Press, Cambridge, MA, 1981).

[23]D. A. Saville, "Electrohydrodynamics: The Taylor–Melcher leaky dielectric model," Annu. Rev. Fluid Mech. **29**, 27–64 (1997).

[24]J. C. Baygents and F. Baldessari, "Electrohydrodynamic instability in a thin fluid layer with an electrical conductivity gradient," Phys. Fluids **10**, 301–311 (1998).

[25]M. H. Oddy, J. G. Santiago, and J. C. Mikkelsen, "Electrokinetic instability micromixing," Anal. Chem. **73**, 5822–5832 (2001).

[26]H. Lin, B. D. Storey, M. H. Oddy, C.-H. Chen, and J. G. Santiago, "Instability of electrokinetic microchannel flows with conductivity gradients," Phys. Fluids **16**, 1922–1935 (2004).

[27]C.-H. Chen, H. Lin, S. K. Lele, and J. G. Santiago, "Convective and absolute electrokinetic instability with conductivity gradients," J. Fluid Mech. **524**, 263–303 (2005).

[28]B. D. Storey, B. S. Tilley, H. Lin, and J. G. Santiago, "Electrokinetic instabilities in thin microchannels," Phys. Fluids **17**, 018103 (2005).

[29]J. D. Posner and J. G. Santiago, "Convective instability of electrokinetic flows in a cross-shaped microchannel," J. Fluid Mech. **555**, 1–42 (2006).

[30]J. D. Posner, C. L. Pérez, and J. G. Santiago, "Electric fields yield chaos in microflows," Proc. Natl. Acad. Sci. **109**, 14353–14356 (2012).

[31]K. Dubey, A. Gupta, and S. S. Bahga, "Coherent structures in electrokinetic instability with orthogonal conductivity gradient and electric field," Phys. Fluids **29**, 092007 (2017).

[32]E. A. Frants, G. S. Ganchenko, V. S. Shelistov, S. Amiroudine, and E. A. Demekhin, "Nonequilibrium electrophoresis of an ion-selective microgranule for weak and moderate external electric fields," Phys. Fluids **30**, 022001 (2018).

[33]G. S. Ganchenko, V. S. Shelistov, E. A. Frants, N. V. Nikitin, S. Amiroudine, and E. A. Demekhin, "Extreme nonequilibrium electrophoresis of an ion-selective microgranule," Phys. Rev. Fluids **4**, 043703 (2019).

[34]G. S. Ganchenko, E. A. Frants, S. Amiroudine, and E. A. Demekhin, "Instabilities, bifurcations and transition to chaos in electrophoresis of charge-selective microparticle," Phys. Fluids **32**, 054103 (2020).

[35]R. F. Probstein, *Physicochemical Hydrodynamics: An Introduction* (Wiley-Interscience, 2003).

[36]R. Courant and D. Hilbert, *Methods of Mathematical Physics: Partial Differential Equations* (Wiley-VCH, New York–London, 1989), Vol. 2.

[37]R. J. Briggs, *Electron-Stream Interaction with Plasmas* (The MIT Press, Cambridge, MA, 1964), p. 204.

[38]A. Bers, "Space-time evolution of plasma instabilities—Absolute and convective," in *Handbook of Plasma Physics*, edited by A. A. Galeev and R. N. Sudan (North-Holland, Amsterdam, 1983), Chap. 3.2, Vol. 1, pp. 451–517.

[39]P. Huerre and P. A. Monkewitz, "Absolute and convective instabilities in free shear layers," J. Fluid Mech. **159**, 151–168 (1985).

[40]P. Huerre and P. A. Monkewitz, "Local and global instabilities in spatially developing flows," Annu. Rev. Fluid Mech. **22**, 473–537 (1990).

[41]H. Schlichting and K. Gersten, *Boundary-Layer Theory* (Springer-Verlag, Berlin, Heidelberg, 2017), p. 805.

[42]C. C. Lin, *The Theory of Hydrodynamic Stability* (Cambridge University Press, Cambridge, 1966), p. 155.

[43]P. G. Drazin, *Introduction to Hydrodynamic Stability* (Cambridge University Press, Cambridge, 2002), p. 258.

[44]M. Gaster, "A note on the relation between temporally-increasing and spatially-increasing disturbances in hydrodynamic stability," J. Fluid Mech. **14**, 222–224 (1962).